The two active glutamates of the plant stress sensor PsbS contribute non-equivalently to its pH-activated molecular response mechanism

Maithili Krishnan[1¶], Patrick E. Konold[2¶], John T.M. Kennis[2*], Anjali Pandit[1,*]

[1] Dept. of Solid-State NMR, Leiden Inst. of Chemistry, Leiden University, Einsteinweg 55, 2300 RA, Leiden, The Netherlands

[2]Department of Physics and Astronomy, Faculty of Science, Vrije Universiteit, De Boelelaan 1081, 1081HV Amsterdam, The Netherlands

[¶]equal contributions

ABSTRACT

The membrane protein Photosystem II subunit S (PsbS) is a pH sensor that plays an essential role in signaling light stress in plants to prevent photo oxidation and generation of detrimental reactive species. PsbS detects thylakoid lumen acidification in excess light conditions via two glutamates facing the lumen, however, its molecular mechanism for activation is elusive. We performed a spectroscopic analysis of wild type *Physcomitrella patens* PsbS and of mutants in which the active glutamates have been replaced (E69Q, E174Q and E69Q / E174Q). We discovered that E69 exerts allosteric control of PsbS dimerization, while E174 is essential for the secondary structural response to low pH. Based on our results, we propose a molecular pH response mechanism that involves a change in the amphiphatic short helix containing E174 facing the lumen, moving from the aqeuous phase into the hydrophobic membrane phase. This structural mechanism may be a shared motif of protein molecular switches of the light-harvesting family and its elucidation could open new routes for crops engineering to improve photosynthetic production of biomass.

Photosynthetic efficiency is tightly coupled with plant fitness under fluctuating environmental conditions, which is prerequisite for survival in a changing global climate. Key to vitality is a continuous balance between light excitation and substrate availability, preventing overload of the electron transfer chain and formation of lethal reactive oxygen species. Overload of the electron-transfer chain in excess light causes acidification of the chloroplast luminal compartments. This provokes a kinetic switch of the photosynthetic antenna into a dimmer state, where excitations are rapidly quenched by a process called Non-Photochemical Quenching (NPQ) (1). Whereas the photo protective feedback response is beneficial for plant fitness, large part of the absorbed solar energy is dissipated during the photo protective state and its transient recovery.

PsbS not only is essential for plant photoprotection, but also offers perspectives for targeted crop engineering. A recent study demonstrated that ~15% increase of crop yield could be achieved in engineered Tobacco plants with increased levels of PsbS that had faster photo protective response kinetics (2). Moreover, raising PsbS levels was shown to increase water use efficiency of tobacco plants(3) and canopy radiation use efficiency in rice plants (4).

The heart of the photo protective mechanism lies in the molecular response to ΔpH. The protein PsbS was identified as gene product required for NPQ activation in plants (5). PsbS acts as a molecular pH-sensor that senses thylakoid lumen acidification and transfers the signal to the antenna, enabling a switch into a photoprotective state via antenna-photosystem rearrangements (6-10) or direct molecular interactions (11-14). PsbS activation involves two lumen-faced Glu residues and may involve a monomerization step (15), although the recently resolved low-pH X-ray structure is a PsbS dimer (16). The molecular response mechanism of PsbS activation is elusive and could not be revealed by crystallography.

We recently introduced strategies for large-scale recombinant production, refolding and dimerization of PsbS for structural characterization (17). Here, we compare the pH-dependent structure and dynamics of wild type (WT) PsbS from *Physcomitrella patens* to that of site-directed glutamate mutants that were shown to have impaired activity in plants *in vivo* to identify the pH-dependent response mechanism.

Three mutants were constructed, E69Q, E174Q and the double mutant E69Q / E174Q PsbS, further denoted as M1 (E69Q), M2 (E174Q) and M3 (E69Q / E174Q). The two active Glu residues E69 and E174 are further

denoted here as E1 and E2. In plants, single mutations of either of the two conserved Glu resulted in reduced NPQ activity, while double mutants would have almost complete abolishment of NPQ (18).

WT PsbS and M1, M2 and M3 were refolded in FC-12 detergent micelles as described earlier (17). Fig.1 present an SDS-page gel electrophoresis analysis of the four samples under pH 7.5 and pH 5.0 conditions. Although denaturing buffer conditions were used, dimer bands are observed, in agreement with previous studies that PsbS can form strong dimers that resist gel denaturation (15, 17). Standard SDS-page using denaturing gel conditions involves a boiling step, which was also omitted here to test the effect on PsbS dimer stability. The figure shows that all the mutants have lower dimer content than the WT. However, the dimer contents vary for the different mutants in the order: dimer content M1 < M3 < M2. Strikingly, mutation of E1 results in the almost complete absence of dimers on gel, indicating strong effect of dimer destabilization.

The dimer contents on gel were slightly increased for the WT at low-pH conditions. The fact that PsbS can form dimers at low and neutral pH has already been confirmed by previous work (17) and agrees with the low-pH crystal structure that is a PsbS dimer.

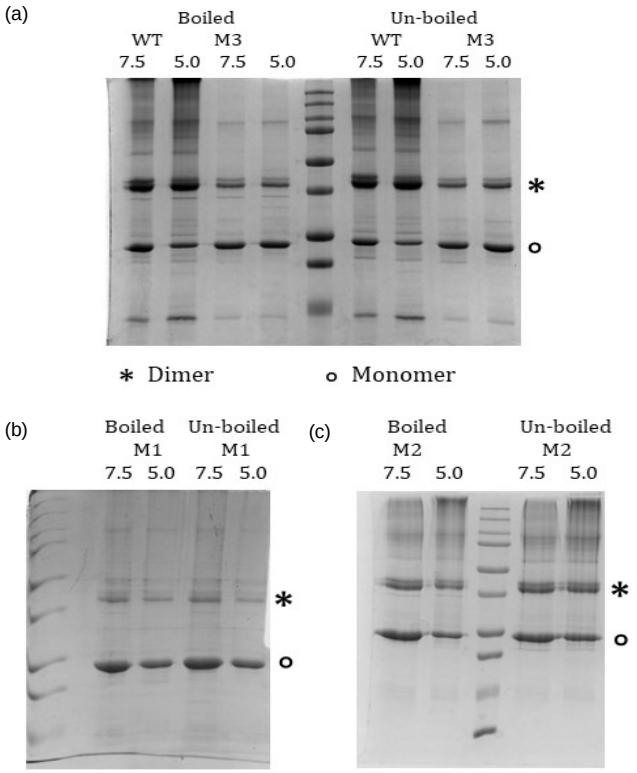

Figure 1. SDS-page analysis of PsbS at pH 7.5 and pH 5.0 conditions. (a) WT PsbS and E69Q / E174Q mutant M3; (b) E69Q mutant M1 and (c) E174Q mutant M2.

To reveal PsbS protonation states at pH 7.5 and 5.0 conditions, *U*-^{13}C-^{15}N WT PsbS and M3 were produced for analysis by solid-state Magic-Angle Spinning (MAS) NMR spectroscopy. Fig. 2 presents the 1D ^{13}C CP MAS spectra of the two samples. Direct ^{13}C polarization MAS NMR was applied, because the dimensions of PsbS in detergent micelles are such that rotational correlation dynamics averages dipolar nuclear couplings, reducing the efficiency of cross-polarization based MAS NMR, while the sizes are too large for detection of rigid protein sites by solution NMR. At pH 7.5, two clear peaks are observed of deprotonated Glu and Asp carboxyl acid side chains. At pH 5.0, these peaks are shifted upfield and overlap with the large ^{13}C' peak centered at 175 ppm of the protein carbonyls, indicating that all the 23 protonatable residues of PsbS are protonated at pH 5.0. The shape of the carbonyl ^{13}C' band of the M3 mutant differs from the WT, which indicates that there are differences between the secondary structure of the WT and the M3 mutant, with more coil structure for the M3 mutant.

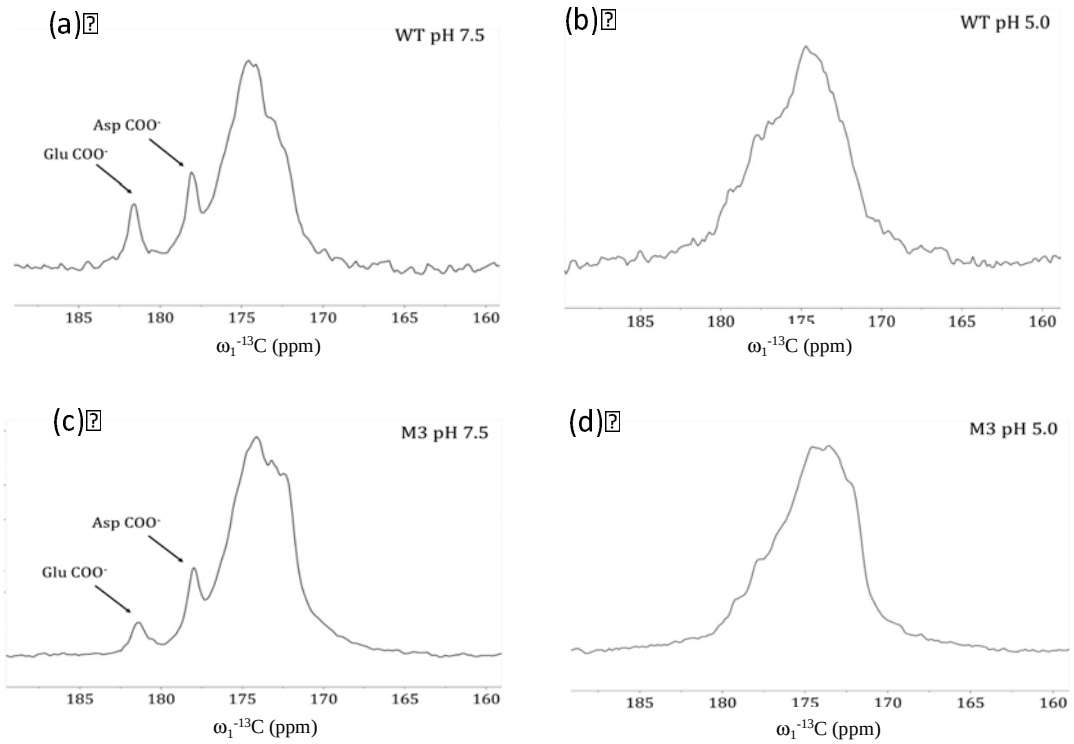

Figure 2. 1D ^{13}C-DP MAS NMR spectra of WT PsbS (a and b) and M3 E69Q / E174Q mutant (c and d) at pH 7.5 (a, c) and pH 5.0 (b, d) conditions.

Fig. 3 shows the FTIR spectra of WT PsbS and of the three mutants at pH 7.5 (orange) and pH 5.0 (green) conditions together with the difference spectrum of pH 5.0 minus pH 7.5 (black). The WT FTIR spectrum at pH

7.5 shows that the Amide I band is centered at 1650 cm^{-1} with a broad shoulder at frequencies up to 1690 cm^{-1} indicative of predominant helical and loop contributions (19), consistent with the X-ray structure (16) and CD data (17). Importantly, the WT spectrum contains a sharp shoulder band at 1630 cm^{-1} that will be discussed below. In addition, the pH 7.5 FTIR spectrum shows a prominent band at 1550 cm^{-1} originating from deprotonated carboxylic acid, representative of deprotonated Glu and Asp residues (20). It does not relate to Amide II, as the protein has been dissolved in D_2O which downshifts the Amide II band by 100 cm^{-1} (21).

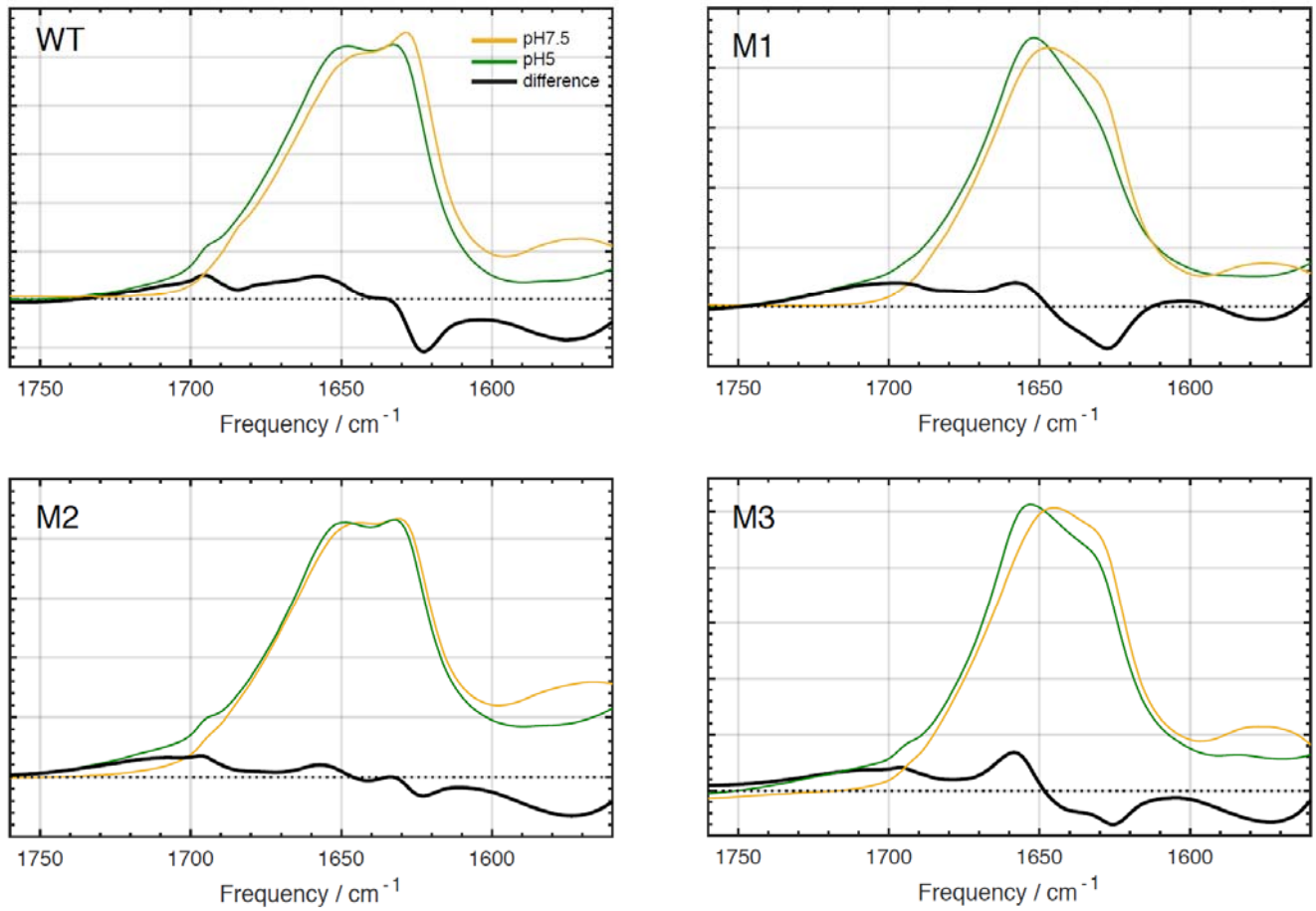

Figure 3. FTIR spectra of WT PsbS, the M1 (E69Q) mutant, the M2 (E174Q) mutant and the M3 (E69Q / E174Q) mutant at pH 7.5 (orange) and pH 5.0 (green) and the difference spectra of pH 5.0 minus pH 7.5 (black). All spectra were taken in D_2O buffer.

At pH 5.0, the 1550 cm^{-1} band is absent while a shoulder from ~1700 to 1750 cm^{-1} is observed in the WT, indicative of protonated carboxyls (20) and demonstrating that all Glu and Asp are protonated at this pH, in agreement with the NMR results. In addition to the protonation effects, the difference spectrum shows a negative

sharp signal at 1625 cm^{-1} and a broad, positive band centered at 1660 cm^{-1}, which may be assigned a change in the Amide I band, and hence to conformational changes in the PsbS secondary structure. The integrated bleach amplitude of the 1625 cm^{-1} band corresponds to 3.6% of the total Amide I absorption, and with a total of 219 amino acids in this construct, hence involves approximately 8 amino acid backbone oscillators.

In the FTIR spectrum of M2, in contrast to the WT spectrum, no prominent changes are observed comparing the two pH conditions except for the carboxyl signals. Notably, the Amide I spectra of M2 under both pH conditions are similar to that of the WT at low pH (Fig. 4).

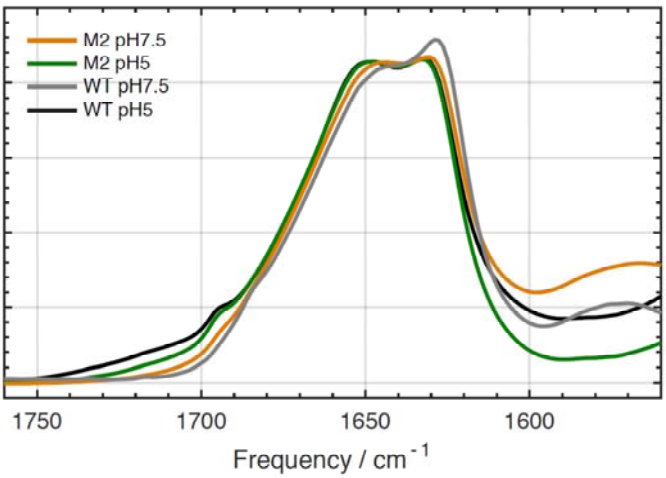

Fig. 4: FTIR spectra of the M2 mutant and wild type PsbS at pH indicated, reproduced from Fig. 3.

The Amide I spectra of M1 and M3 mutant do not resemble the WT spectra at either pH conditions, consistent with the fact that the NMR $^{13}C'$ signal of the M3 differed from that of the WT at both pH. We conclude that mutation of E1 affects the secondary structure of PsbS. The difference spectra of M1 and M3 show in the amide I region well-resolved positive band at 1660 cm^{-1} and negative signal intensities between 1625-1640 cm^{-1}.

Combining the results, we can conclude that the most prominent structural change of PsbS going from neutral to low pH consists of loss of a characteristic band at 1625 cm^{-1} and that this effect is strongly inhibited by mutation of E2. The difference spectrum of M3 shows that if both active Glu are mutated, conformational changes occur that are not present in the WT and that must be induced by protonation of other protonatable residues at low pH. Indeed, both the IR and NMR data show that going from pH 7.5 to pH 5.0 all the protonatable Asp and Glu residues undergo a change in protonation state.

Two-dimensional IR spectroscopy (2DIR) can shed further light on the FTIR results. The steady-state 2DIR spectrum of wild-type PsbS at pH 7.0 is presented in Fig. 5A, along with the linear spectrum (upper panel). It exhibits spectral congestion as typically observed in several other protein systems due to the overlapping Amide I contributions of several structural elements (22). Adjacent to the negative bleach bands along the diagonal, reflecting depopulation of ground state modes $v = 0 \longrightarrow 1$, we observed corresponding anharmonic satellite peaks of positive sign, corresponding to the $v = 1 \longrightarrow 2$ transition and slightly red-shifted along Ω_{emis}.

We recorded 2DIR spectra at pH 7.5 and pH 5.0, and determined the difference spectrum (Fig. 5B), thereby scaling the 2DIR spectra on the integrated Amide I absorption between 1610 and 1690 cm^{-1} of both samples. The FTIR difference spectrum is shown in the upper panel. The 2DIR difference spectrum shows significantly less spectral congestion as several discrete peaks are observed, indicating that specific conformational changes take place. Beginning on the low frequency side, there is a $v = 0 \longrightarrow 1$, $v = 1 \longrightarrow 2$ peak pair centered at ~1630 cm^{-1}, coinciding with the negative feature identified in the difference FTIR spectrum at 1625 cm^{-1}. The 5 cm^{-1} difference in their respective maxima likely result from compensation by positive signals at the high-frequency side in the FTIR difference spectrum, as can also be deduced from the asymmetric lineshape of the 1625 cm^{-1} bleach. Accordingly, the sign of the 1630 cm^{-1} band in 2DIR reflects population loss with the positive lobe falling on the diagonal. This signal thus represents loss of a specific secondary structure element. Two diagonal peak pairs of opposite sign with respect to that at 1630 cm^{-1} lie at 1638 and 1660 cm^{-1}, which indicates that these pairs represent population gain of two distinct secondary structure elements. A strong cross peak [1630,1660] lies between the highest and lowest diagonal bands.

The nature of the 1630 cm^{-1} transition warrants further attention since this frequency falls on the boundary expected for α-helical and β-sheet amide I oscillators (19). The band anharmonicity of the 1630 cm^{-1} transition amounts to $\Delta = 13$ cm^{-1}, which implies it corresponds to an ordered secondary structure element, as Δ inversely scales with the degree of excitonic coupling (23), and uncoupled Amide I oscillators give Δ values of 16 cm^{-1} (24). β-sheets exhibit a characteristic "Z-shaped" peak pattern (25) which is not observed here, and we hence conclude that the 1630 cm^{-1} feature corresponds to a helical element. This agrees with the X-ray structure and CD data which indicate no extensive β-sheet content (16, 17). A similar reasoning may be applied to the two band

pairs at 1638 and 1660 cm^{-1}, which show band anharmonicity similar to that at 1630 cm^{-1}, no Z-shape 2DIR pattern and thus indicate gain of two distinct helical elements.

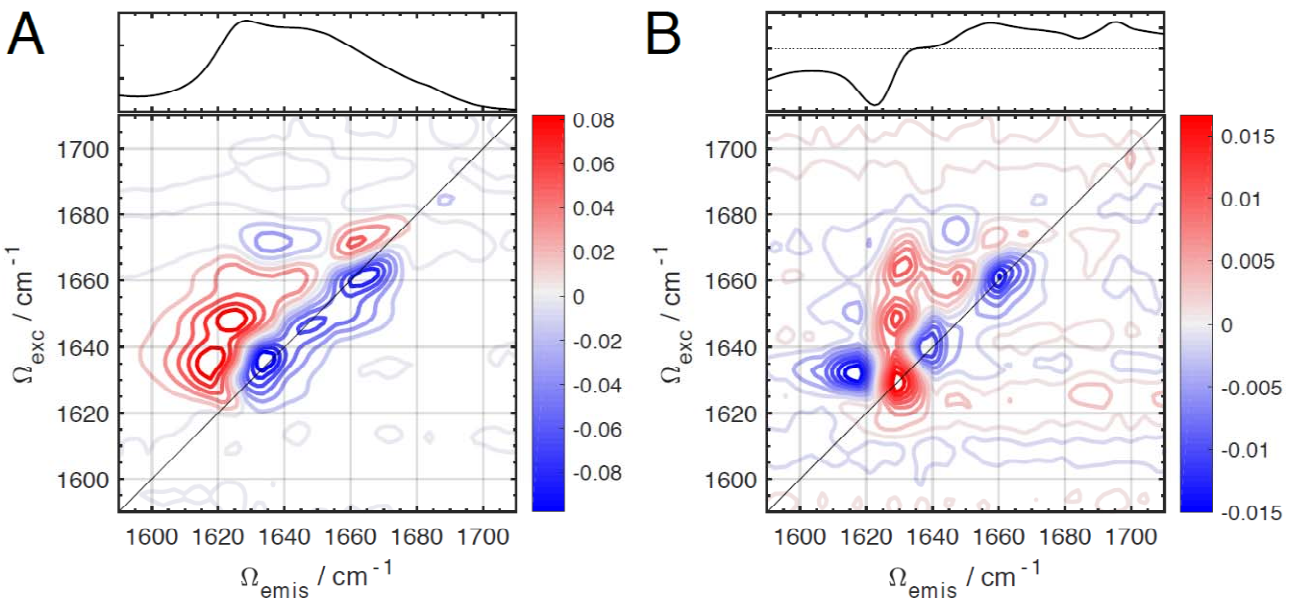

Figure 5. (A) Steady-state 2DIR correlation spectrum at T=400 fs of wild-type PsBs in pH7 buffer. (B) pH 5.0 – pH 7.5 difference 2DIR of wild-type PsbS.

An additional useful means to gain molecular insight from 2DIR spectra lies in the slope of the nodal line (NLS). This quantity is proportional to the vibrational energy gap frequency-frequency correlation function (FFCF) and reports on the degree of vibrational inhomogeneity of the system (26-28). the band pair at 1630 cm^{-1} has a NLS parallel to the Ω_{exc} axis, which indicates a highly homogeneous structure. In contrast, the band at 1638 cm^{-1} has a NLS nearly parallel to the diagonal, representing a case with large heterogeneity. The 1660 cm^{-1} band pair demonstrates a NLS between the former examples, which can be interpreted as a case with intermediate heterogeneity. Our interpretation of the difference 2DIR results, considering their frequency, anharmonicity, inhomogeneity, and sign, is as follows:

i) the 1630 cm^{-1} diagonal peak reflects loss of a single helical element in a homogeneous environment and corresponds to the loss observed in the difference FTIR spectra. The low frequency of 1630 cm^{-1} of this helical element strongly indicates that it has a high degree of exposure to the aqueous solvent (29, 30).

ii) the 1638 cm^{-1} diagonal peak represents gain of a helical element that exhibits a significant degree of conformational disorder.

iii) the 1660 cm^{-1} diagonal peak represents gain of a helical element with an intermediate degree of conformational disorder.

iv) the prominent [1630,1660] cross peak most likely results from a loss of coupling between the ordered helical element that exists at pH 7.0 with adjacent Amide I elements at 1660 cm^{-1}.

To interpret the observed pH-dependent structural changes, we turn to the crystal structure of PsbS, which represents the PsbS at low pH (16). In the structure, the conserved Glu E1 (E69) is located in a luminal loop that connect two transmembrane helices TM1 and TM2 whereas E2 (E174) is located in the amphiphatic short helix H2 at the water-membrane interface facing the lumen. In the spinach PsbS structure, the carbonyl and carboxyl CO group of E2 each can forms a hydrogen bond with two backbone amides of Ile74 and Tyr75 in the luminal loop of the adjacent monomer. In *P. patens* PsbS, those two amino acids Leu74 and Thr75. Fig. 6 shows a schematic picture of the PsbS dimer side facing the lumen. At the lumen site, the dimer is stabilized by four hydrogen bonds, connecting E2 of monomer 1 to the luminal loop of monomer 2 and *vice versa*.

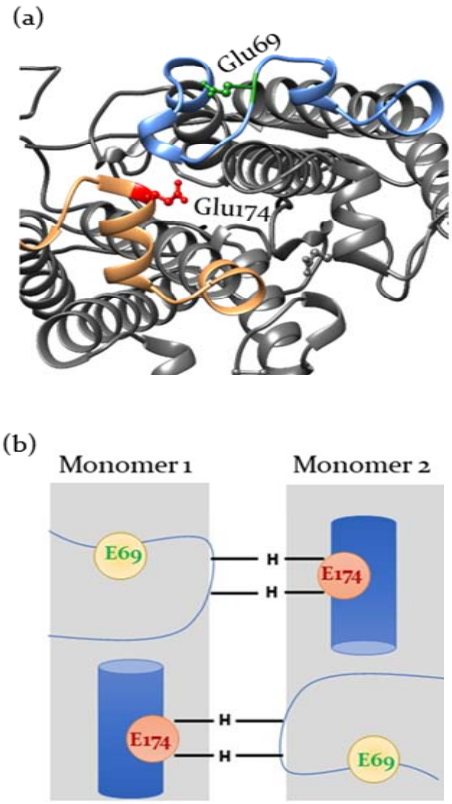

Figure 6. (a) Homology model of *P. patens* PsbS dimer showing the lumen site with the two active Glu, E69 and E174. (b) Schematic picture of dimer-stabilizing hydrogen bonds at the lumen site, involving E174 and the loop containing E69.

The M1 mutant is strongly impaired in dimerization although E1 is not close to the dimer interface and in fact, is at the exterior site of the PsbS dimer. The E1 residue is part of the luminal loop that is connected to E2 of the adjacent monomer via two hydrogen bonds. The highly reduced dimer content of M1 suggests that the site of E1 has an allosteric effect on the dimerization of PsbS. Substitution of this residue by Gln could re-orient the luminal loop, disrupting the the inter-monomer hydrogen bonds to E2.

The M2 mutant is still capable of dimer formation, even though this mutant lacks E2 that is involved in forming two inter-monomer hydrogen bonds via its carboxyl and carbonyl. This can be explained since in M2, E2 is substituted for Gln, which contains a side chain carbonyl that is capable of hydrogen bonding, whilst the other H bond may be formed to the backbone carbonyl.

We now discuss the origin of the Amide I difference signals observed in FTIR and 2DIR spectroscopy, which indicate conformational changes in the secondary structure. In FTIR, we observe a distinct negative/positive Amide I signal at 1625 (-) / 1660 (+) cm^{-1} in WT PsbS (Fig. 3). This signal is also reflected and refined in 2DIR spectroscopy, where loss of a helical signal at 1630 cm^{-1} is accompanied by gain of helical signal at 1638 cm^{-1} and 1660 cm^{-1} (Fig. 5). Strikingly, mutation of M2 almost completely abolishes the structural Amide I response of PsbS to low pH (Fig. 3). This observation reveals that the lumen-facing amphiphatic helix H2 containing E2 likely represents the site of plasticity that undergoes a pH-dependent structural change and is responsible for the characteristic 1625 cm^{-1} signal. Notably, the amplitude of this difference signal corresponds to approximately 8 amino acids, which agrees with the length of this helix in the X-ray structure (9 amino acids) (16). The 2DIR spectra on the WT indicate that the 1630 cm^{-1} signal represents a highly ordered helical element that transforms into two distinct, less-ordered helical elements at 1638 and 1660 cm^{-1}.

Low-pH PsbS crystals that were soaked with DCCD show its binding to E2, indicating that in the low-pH conformation, this Glu residue is in a hydrophobic environment (16). Because E2 is negatively charged at neutral pH, it is expected that at pH 7.5, the polar site of the amphiphatic helix H2 containing E2 will be stabilized at the aqueous environment of the lumen, consistent with its low frequency (1630 cm^{-1}) at that pH. Protonation of E2 at

low pH therefore could move the helix from the water towards or into the membrane phase, which is consistent with the higher frequencies of the helical elements at pH 5.0 observed at 1638 and 1660 cm^{-1}.

In the M2 mutant, the charge at the E2 site is neutralized by the Glu to Gln mutation, which predicts that M2 PsbS will already adopt a low-pH conformation at neutral pH. This is exactly what is observed, since the amide I spectrum of M2 at both pH conditions resembles the low-pH spectrum of the WT.

The IR spectrum of M1 does not resemble the WT IR spectrum at low pH, neither does it reflect the WT spectrum at neutral pH, indicating that part of the M1 PsbS adopts a non-native fold. The luminal loop containing E1 contains an additional conserved, second Glu close to TM2, E76, and, for *P. patens* PsbS, also contains an Asp residue (Asp67). At neutral pH, those residues will have negative charge, while in M1 and M3 E1 is neutralized by Gln, resulting in a charge distribution along the luminal loop stretch that neither reflect the luminal loop charges of WT PsbS at neutral pH, nor reflects the loop charges of the WT at low pH conditions. This may lead to a non-native fold of the luminal loop stretch in M1 and M3, accounting for the difference in secondary structure compared to the WT. The collective effect of E1 and E2 mutation may produce a moderated PsbS structure, in which the substituted Gln at the E2 helix site is capable of interacting with the modified loop of the adjacent monomer, which could explain why dimers are more stabilized in M3 than in M1.

Summarizing, we discovered that the two active Glu sites respond nonequivalently to low pH. The luminal loop containing E1 has an allosteric effect on PsbS dimerization. E2 is responsible for the structural response of PsbS to changes in pH, most likely by a movement of the amphiphatic short helix fragment H2 towards/into the membrane phase, thereby becoming significantly less ordered. Single-point mutations of E1 and E2 in PsbS have been reported to severely reduced NPQ activity (18), implicating that both dimerization and flexibility of the amphiphatic short helix stretch are important for PsbS function. The M2 mutant represents the low-pH state of PsbS, which is the active state. Reduced NPQ activity of this mutant in plants suggests that not the activation of PsbS, but its ability to switch on and off is crucial for its function. Indeed, PsbS is not only involved in switching on NPQ, but also essential for rapid de-activation and recovery of this process in fluctuating light conditions.

PsbS is a member of the Light Harvesting Complex (LHC) family, of which proteins form pH switches (PsbS and LHCSR) and photoprotective switches that can alternate between fluorescent and excitation-quenched states (LHCII and LHCSR). LHCs share a structure in which transmembrane helices are connected via amphiphatic

short helices at the luminal site. Responsiveness of the amphiphatic helices to changes in pH, hydrophobicity or other alterations in the physico-chemical environment might be a common motif that enables LHCs to operate as molecular controls for regulating photosynthetic light harvesting.

Materials and Methods

Mutants creation Three plasmids of mutant patens PsbS were purchased from Baseclear B.V.® Single mutants with E69Q and E174Q were named as M1 and M2. A double mutant with E69Q and E174Q was created and named as M3. These plasmids were transformed, and the mutant proteins were overexpressed and purified as described for the WT in (17). PsbS WT and the three mutants were refolded in FC-12 detergent buffer at pH 5.0 and pH 7.5 conditions.

Gel electrophoresis SDS-page gel electrophoresis analysis (12.5% running gel, 4% stacking gel stained with Coomassie brilliant blue R-250 Bio-Rad) was carried out for checking the yield of PsbS at every step of overexpression, purification and refolding. 2.5µL of Precision Plus Protein™ Dual Color Standard from Sigma was used in every SDS-page gel.

NMR spectroscopy Solid-state NMR measurements were performed on a Bruker Avance I 750-MHz wide-bore solid-state NMR spectrometer with 17.6 Tesla magnetic field. In this field, ^{13}C and ^{1}H resonate at 188.66 and 750.23 MHz respectively. Standard 4 mm triple resonance MAS probe was used. All the samples were packed in 4mm zirconium rotors with top insert and were spun at the magic angle (54.74^0). The spinning frequency was set at 13 kHz. The temperature was set at 293 K.

^{13}C spectra were obtained through direct polarization also referred to as 'hpdec'. 90^0 or ($\pi/2$) carbon pulses of 6.2 µs and 3.1 µs proton pulses were applied. An acquisition time of 36.2 ms was used. For the experiments, 10000 scans were acquired with a constant recycle delay of 5 s. A line broadening function of 50 Hz was applied for processing the spectra. All the ^{13}C spectra were externally referenced to methyl signal of tetramethylsilane (TMS).

FTIR spectroscopy Infrared difference spectra were recorded using an FTIR spectrometer (IFS 66s Bruker) equipped with a nitrogen-cooled photovoltaic Mercury Cadmium Telluride (MCT) detector (20 MHz, KV100, Kolmar Technologies) described earlier (31). The samples were contained between CaF_2 windows separated with a 20 µm Teflon spacer for D_2O buffer and the concentration was tuned for OD ~0.8 absorptions at 1650 cm^{-1}. The measurements were carried out at room temperature and spectral resolution of the instrument was 3 cm^{-1}.

2DIR spectroscopy Two-dimensional infrared spectroscopy (2DIR) was carried out in the pump-probe geometry as previously described (32, 33), as an extension to an existing femtosecond mid-IR spectrometer (34). In short, femtosecond midIR pulses were generated via difference frequency generation in Ag_2GaS_2 (100 fs pulse duration, 200 cm^{-1} bandwidth) pumped by a Ti:sapphire regenerative amplifier with 1 kHz repetition rate. A 5% fraction was split off for the probe beam with a wedged CaF_2 window. The pump beam was modulated with a germanium acousto-optic modulator (Quickshape, PhaseTech, Madison WI). Data was collected in the time domain by oversampling along the free induction decay (τ) in the rotating frame with a two-pulse, four-frame phase-cycling scheme to isolate the $\chi^{(3)}$ response and remove contributions from scattered pump light *in situ*. The pump and probe beams were focused on the sample with an off-axis parabolic mirror, overlapped in space, and set to a designated delay using a motorized linear delay stage. The transmitted probe beam was collimated and detected with a 64-element Mercury Cadmium Telluride (MCT) photodiode array (Infrared Associates). A parallel polarization condition <ZZZZ> was employed by tuning the polarization of the pump beam with a combination $\lambda/2$ MgF_2 waveplate (Karl Lambrecht) and wire-grid polarizer (Thorlabs). The PsbS samples were contained between two CaF_2 windows separated with a 20 µm Teflon spacer. D_2O buffer solution was used to minimize the background absorption. Measurements with the pH 5.0 and 7.5 samples were collected consecutively and difference 2DIR spectra were produced by scaling according to the integrated linear absorption of the amide I band (1610 – 1690 cm^{-1}).

ASSOCIATED CONTENT

Supporting Information. Overlaid FTIR spectra of wild type and M2 mutant PsbS are shown in the Supporting Information section.

AUTHOR INFORMATION

Corresponding Author

a.pandit@chem.leidenuniv.nl; j.t.m.kennis@vu.nl

ACKNOWLEDGMENT

Dr. Karthick Sai Sankar Gupta is greatly acknowledged for assistance with the NMR spectroscopy.

REFERENCES

1. Ruban AV, Johnson CDP, & Duffy (2012) The photoprotective molecular switch in the photosystem II antenna. *Biochimica et biophysica acta. Bioenergetics* 1817(1):167-181.
2. Kromdijk J*, et al.* (2016) Improving photosynthesis and crop productivity by accelerating recovery from photoprotection. *Science* 354(6314):857.
3. Glowacka K*, et al.* (2018) Photosystem II Subunit S overexpression increases the efficiency of water use in a field-grown crop. *Nature communications* 9(1):868.
4. Hubbart S*, et al.* (2018) Enhanced thylakoid photoprotection can increase yield and canopy radiation use efficiency in rice. *Communications Biology* 1(1):22.
5. Niyogi KK & Truong TB (2013) Evolution of flexible non-photochemical quenching mechanisms that regulate light harvesting in oxygenic photosynthesis. *Current Opinion in Plant Biology* 16(3):307-314.
6. Goral TK*, et al.* (2012) Light-harvesting antenna composition controls the macrostructure and dynamics of thylakoid membranes in Arabidopsis. *The Plant Journal* 69(2):289-301.
7. Ikeuchi M, Uebayashi N, Sato F, & Endo T (2014) Physiological Functions of PsbS-dependent and PsbS-independent NPQ under Naturally Fluctuating Light Conditions. *Plant and Cell Physiology*.
8. Kiss A, Ruban A, & Horton P (2008) The PsbS Protein Controls the Organization of the Photosystem II Antenna in Higher Plant Thylakoid Membranes. *Journal of biological chemistry* 283(7):3972-3978.
9. Ware MA, Belgio E, & Ruban AV (2015) Comparison of the protective effectiveness of NPQ in Arabidopsis plants deficient in PsbS protein and zeaxanthin. *Journal of Experimental Botany* 66(5):1259-1270.
10. Wobbe L, Bassi R, & Kruse O (Multi-Level Light Capture Control in Plants and Green Algae. *Trends in Plant Science* 21(1):55-68.
11. Correa-Galvis V, Poschmann G, Melzer M, Stühler K, & Jahns P (2016) PsbS interactions involved in the activation of energy dissipation in Arabidopsis. *Nature Plants* 2:15225.
12. Dall'Osto L*, et al.* (2017) Two mechanisms for dissipation of excess light in monomeric and trimeric light-harvesting complexes. *Nature Plants* 3:17033.
13. Gerotto C, Franchin C, Arrigoni G, & Morosinotto T (2015) In Vivo Identification of Photosystem II Light Harvesting Complexes Interacting with PHOTOSYSTEM II SUBUNIT S. *Plant Physiology* 168(4):1747-1761.
14. Sacharz J, Giovagnetti V, Ungerer P, Mastroianni G, & Ruban AV (2017) The xanthophyll cycle affects reversible interactions between PsbS and light-harvesting complex II to control non-photochemical quenching. *Nature Plants* 3:16225.
15. Bergantino E*, et al.* (2003) Light- and pH-dependent structural changes in the PsbS subunit of photosystem II. *Proceedings of the National Academy of Sciences of the United States of America* 100(25):15265-15270.
16. Fan M*, et al.* (2015) Crystal structures of the PsbS protein essential for photoprotection in plants. *Nature Structural &Amp; Molecular Biology* 22:729.
17. Krishnan M, Moolenaar GF, Gupta K, Goosen N, & Pandit A (2017) Large-scale in vitro production, refolding and dimerization of PsbS in different microenvironments. *Sci Rep* 7(1):15200.
18. Li XP*, et al.* (2004) Regulation of photosynthetic light harvesting involves intrathylakoid lumen pH sensing by the PsbS protein. *The Journal of biological chemistry* 279(22):22866-22874.
19. Krimm S & Bandekar J (1986) VIBRATIONAL SPECTROSCOPY AND CONFORMATION OF PEPTIDES, POLYPEPTIDES, AND PROTEINS. *Advances in Protein Chemistry* 38:181-364.

20. Barth A (2000) The infrared absorption of amino acid side chains. *Prog. Biophys. Mol. Biol.* 74(3-5):141-173.
21. Blout ER, Deloze C, & Asadourian A (1961) DEUTERIUM EXCHANGE OF WATER-SOLUBLE POLYPEPTIDES AND PROTEINS AS MEASURED BY INFRARED SPECTROSCOPY. *Journal of the American Chemical Society* 83(8):1895-&.
22. Ganim Z*, et al.* (2008) Amide I two-dimensional infrared Spectroscopy of proteins. *Accounts of Chemical Research* 41(3):432-441.
23. Zhao J & Wang JP (2012) Chain-length and mode-delocalization dependent amide-I anharmonicity in peptide oligomers. *Journal of Chemical Physics* 136(21).
24. Wang JP & Hochstrasser RM (2006) Anharmonicity of amide modes. *Journal of Physical Chemistry B* 110(8):3798-3807.
25. Demirdoven N*, et al.* (2004) Two-dimensional infrared spectroscopy of antiparallel beta-sheet secondary structure. *Journal of the American Chemical Society* 126(25):7981-7990.
26. Eaves JD*, et al.* (2005) Hydrogen bonds in liquid water are broken only fleetingly. *Proceedings of the National Academy of Sciences of the United States of America* 102(37):13019-13022.
27. Kwac K & Cho MH (2003) Molecular dynamics simulation study of N-methylacetamide in water. II. Two-dimensional infrared pump-probe spectra. *Journal of Chemical Physics* 119(4):2256-2263.
28. Guo Q, Pagano P, Li YL, Kohen A, & Cheatum CM (2015) Line shape analysis of two-dimensional infrared spectra. *Journal of Chemical Physics* 142(21).
29. Byler DM & Susi H (1986) EXAMINATION OF THE SECONDARY STRUCTURE OF PROTEINS BY DECONVOLVED FTIR SPECTRA. *Biopolymers* 25(3):469-487.
30. Reisdorf WC & Krimm S (1996) Infrared amide I' band of the coiled coil. *Biochemistry* 35(5):1383-1386.
31. Alexandre MTA, van Grondelle R, Hellingwerf KJ, & Kennis JTM (2009) Conformational Heterogeneity and Propagation of Structural Changes in the LOV2/J alpha Domain from Avena sativa Phototropin 1 as Recorded by Temperature-Dependent FTIR Spectroscopy. *Biophysical Journal* 97(1):238-247.
32. Shim S-H, Strasfeld DB, Ling YL, & Zanni MT (2007) Automated 2D IR spectroscopy using a mid-IR pulse shaper and application of this technology to the human islet amyloid polypeptide. *Proceedings of the National Academy of Sciences of the United States of America* 104(36):14197-14202.
33. Shim S-H & Zanni MT (2009) How to Turn Your Pump-Probe Instrument Into a Multidimensional Spectrometer: 2D IR and Vis Spectroscopies via Pulse Shaping. *Physical Chemistry Chemical Physics* 11(5):748-761.
34. Konold PE*, et al.* (2016) Unfolding of the C-Terminal J alpha Helix in the LOV2 Photoreceptor Domain Observed by Time-Resolved Vibrational Spectroscopy. *Journal of Physical Chemistry Letters* 7(17):3472-3476.